Critical behavior of the random-field Ising magnet with long-range correlated disorder

Björn Ahrens* and Alexander K. Hartmann
Institute of Physics, University of Oldenburg, D-26111 Oldenburg, Germany
(Received 30 June 2011; revised manuscript received 5 September 2011; published 7 October 2011)

We study the correlated-disorder-driven zero-temperature equilibrium phase transition of the random-field Ising magnet (RFIM) using exact numerical ground-state calculations for cubic lattices. We consider correlations of the quenched disorder decaying proportionally to r^a, where r is the distance between two lattice sites and $a < 0$. To obtain exact ground states, we use a well-established mapping to the graph-theoretical maximum-flow problem, which allows us to study large system sizes of more than 2×10^6 spins. We use finite-size-scaling analyses for values $a = \{-1, -2, -3, -7\}$ to calculate the critical point and the critical exponents characterizing the behavior of the specific heat, magnetization, susceptibility, and the correlation length close to the critical point. We find basically the same critical behavior as for the RFIM with δ-correlated disorder, except for the finite-size exponent of the susceptibility and for the case $a \geqslant -2$, where the results are also compatible with a phase transition at infinitesimal disorder strength. We numerically confirm earlier predictions.

DOI: 10.1103/PhysRevB.84.144202 PACS number(s): 64.60.De, 75.10.Nr, 75.40.−s, 75.50.Lk

I. INTRODUCTION

The random-field Ising magnet (RFIM) is a prototypical model for magnetic systems with quenched disorder. For $d = 3$ and higher dimensions,[1] it is known in equilibrium to undergo a second-order phase transition[2–13] at a critical temperature T_c or disorder strength h_c [$T_c(h) \Leftrightarrow h_c(T)$]: For low temperatures and weak disorder the ferromagnetic interactions dominate and the system is long-range ordered. For high temperature or strong disorder, the RFIM exhibits no long-range order and behaves like a paramagnet in a field.

The quenched disorder used in earlier studies of the RFIM was mostly uncorrelated (δ correlated).[2–12] This is quite common in the literature when disordered systems like percolation, random ferromagnets, spin glasses, or polymers in random media are studied. Nevertheless, real systems are always emerging from physical processes; hence correlations are present, which could play an important role in the behavior of the RFIM. Here, we consider a tunable, scale-free (power-law), i.e., long-range, correlation to the random field to explore its influence on the critical behavior. Please note that for an exponentially decreasing correlation strength with a typical length scale Ξ, via renormalizing the system beyond Ξ, the behavior of the uncorrelated system should be recovered. The $O(n)$ random-field model with long-range correlated disorder was studied recently[14] via functional renormalization group methods around $d = 4$ and for values $n > 3$, i.e., without including the Ising case $n = 1$. Furthermore, Nattermann[15] considered an Ising model with long-range-correlated disorder by means of an Imry-Ma argument and its effects on the lower critical dimension; for details, see the end of this section.

For other types of random system, there exist already some studies for the case of long-range-correlated disorder, e.g., for percolation,[16] the diluted Ising ferromagnet,[17] random walks,[18] or elastic systems.[19]

Now, we state our model in detail. The RFIM consists of Ising $N = L^3$ spins $S_i = \pm 1$ located on the sites of a cubic lattice with periodic boundary conditions in all directions. The spins couple to each other and to local net fields. Its Hamiltonian reads

$$\mathcal{H} = -J \sum_{\langle i,j \rangle} S_i S_j - \sum_i (h\eta_i + H) S_i. \tag{1}$$

It has two contributions. The first covers the spin-spin interaction, where J is the ferromagnetic coupling constant between two adjacent spins and $\langle i,j \rangle$ denotes pairs of next-neighbour spins. The second part of the Hamiltonian describes the coupling to local and global fields $h\eta_i$ and H, respectively. The factor h is the disorder strength used to trigger the phase transition. In $d > d_l = 2$ the system is ferromagnetically ordered for small temperatures T and below the critical disorder strength $h < h_c(T)$, while in all other cases it is a paramagnet in a field. The global field is included only for technical reasons to calculate the susceptibility in the limit $H \to 0$. The quenched local fields η_i are Gaussian distributed with zero mean and unit standard deviation. The important property of these fields is their spatial long-range correlation. It decays as a power law

$$\mathcal{C}(\vec{r}) \equiv \left\langle \frac{1}{N} \sum_{\vec{x}} \eta(\vec{x})\eta(\vec{x}+\vec{r}) \right\rangle \sim |\vec{r}|^a \tag{2}$$

with a tunable, well-defined decay exponent a. The symbol $\langle \cdots \rangle$ denotes the average over the quenched disorder. $\vec{x}$ is the position of a lattice site i.

We will study the equilibrium behavior (using exact ground-state calculations) in particular for the values $a = \{-1.0, -2.0, -2.5, -3.0, -7.0\}$. First of all, it is interesting to know whether this type of disorder is relevant with respect to the ordered case. It was shown by Nattermann[15] explicitly for the RFIM, but also for systems with "random-temperature disorder" like the diluted ferromagnet,[20] that for a d-dimensional system the behavior of uncorrelated quenched disorder is recovered if $|a| > d$, i.e., when the disorder correlation vanishes faster than the system grows. The usual Harris criterion applies.[20] It states[21] that the disorder is relevant if $d\nu - 2 < 0$, ν being the critical exponent of the ordered system. For the $d = 3$ ferromagnet $\nu = 0.6294(5)$ (see Ref. 22); hence the disorder is relevant, as is known from the uncorrelated disorder. Furthermore, the study of Natterman predicts, using an extended Imry-Ma argument, that extremely long-range correlations of the disorder with $0 < |a| \leqslant 2$ lead to a domain state which destroys long-range ferromagnetic order, i.e., $h_c = 0$. Finally, for $2 < |a| < 3$ domain wall roughening occurs, which means that the critical

 ©2011 American Physical Society

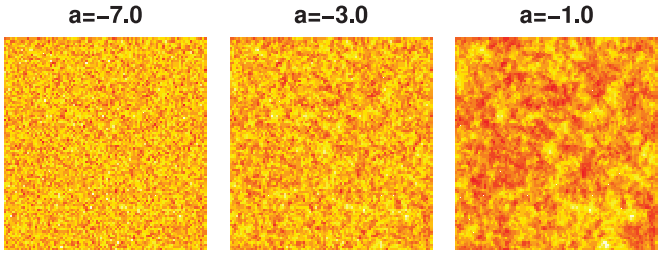

FIG. 1. (Color online) Slices of the same correlated disorder of a 97^3 lattice for different correlation exponents. The random fields are heat coded. Bright means high positive field and dark means high negative field.

behavior of the RFIM might be altered with respect to the uncorrelated case.

The results we present in this work are to a large extent compatible with these predictions: Our results show that the most exponents are compatible within error bars with the values of the standard RFIM for all values of the correlation exponent a. Nevertheless, the combination γ/ν shows a clear signature of nonuniversality for $a \geqslant -3$. This is similar to the diluted Ising model, where the long-range-correlated dilution clearly changes some but not all critical exponents[17] with respect to the uncorrelated case.[23]

The paper is organized as follows: In Sec. II we sketch the method of calculation of Gaussian-distributed correlated random numbers. After that a brief description of the numerical ground-state approach is given. The measured quantities and the methods used to analyze the data are displayed in Sec. III. Our numerical results are presented in Sec. IV. Based on the results we discuss the extremes of correlated disorder. The last section contains the discussion and conclusions.

II. NUMERICAL METHODS

In this section, we first explain how we generated the samples of correlated disorder. Second, we briefly outline the numerical approach used to calculate the exact ground states of these samples.

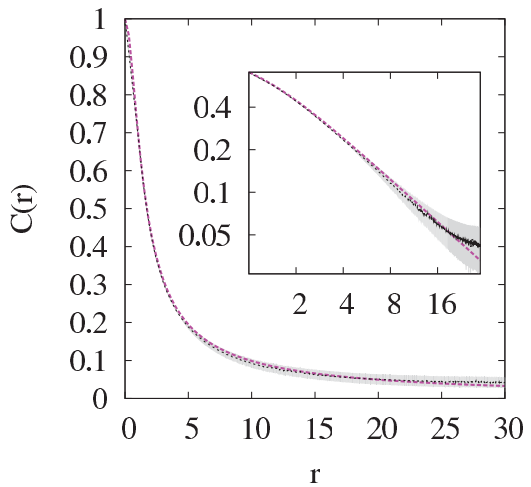

FIG. 2. (Color online) Mean of the two-point correlations for 20 arbitrary samples of long-range-correlated random fields for $L = 49, a = -1$ (black line) and error (gray background). The dashed (magenta) line is a fit according to Eq. (3) with $a = 1.003(2)$. The inset shows the same data as a log-log plot.

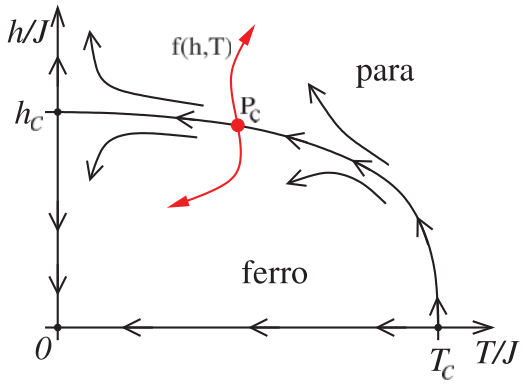

FIG. 3. (Color online) Schematic diagram of the phase space of the RFIM. The path $f(h,T)$ (red line) shows an arbitrary path crossing the phase boundary. The small arrows denote the renormalization group flow.

To obtain a realization of correlated random fields, we basically apply the ideas of Refs. 20, 16, and 17. The recipe is to search for a convolution kernel $\Phi(\vec{r})$ which convolves independent and identically distributed (iid) random numbers $u(\vec{r})$, such that $\eta(\vec{r}) = \Phi(\vec{r}) * u(\vec{r}) = \sum_{\vec{x}} \Phi(\vec{x}) u(\vec{r} - \vec{x})$ show a desired two-point correlation with periodic boundary conditions for $u(\cdot)$. Power-law correlations are created, using

$$C(\vec{r}) = (1 + |\vec{r}|^2)^{a/2}, \quad a < 0. \tag{3}$$

The long-range behavior is the same as that of a pure power law without a singularity at the origin. This avoids a zero-mode divergence.[24,25]

In Fourier space the correlation function is equivalent to the spectral density. The transformation $\mathcal{F}$ is given through $\tilde{\eta}(\vec{k}) \equiv \sum_{\vec{x}} e^{i\vec{k}\cdot\vec{x}} \eta(\vec{x})$. Application of the definition of $C(\vec{r})$ from Eq. (2) results in

$$\langle \tilde{\eta}(\vec{k}) \tilde{\eta}^*(\vec{k}) \rangle = \left\langle \sum_{\vec{r}} e^{i\vec{k}\cdot(\vec{x}+\vec{r})} \eta(\vec{x}+\vec{r}) \sum_{\vec{x}} e^{-i\vec{k}\cdot\vec{x}} \eta(\vec{x}) \right\rangle = N \tilde{C}(\vec{k}). \tag{4}$$

TABLE I. Number of disorder realizations per system size and correlation exponent in thousands (10^3) and the external field H_1, used to calculate the susceptibility.

L	$a=-1$	$a=-2$	$a=-2.5$	$a=-3$	$a=-7$	H_1
7	33	33	674	33	33	0.0075
11	33	33	440	33	33	0.0050
15	13	32	420	61	182	0.0030
21		29	235	14	155	0.0025
25	90	32	235		150	0.0015
35	44	10	420	45	14	0.0015
49	32	26	231	16	16	0.0010
69	16	24	104	9	15	0.0005
97	20	8	265	4.5	9.5	0.0004
117	3	1	48	1.2	1.8	0.0002
141	1	0.2	1.3	0.2	0.3	0.0001

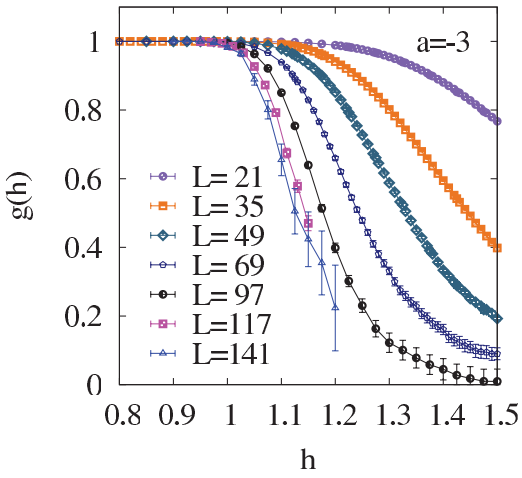

FIG. 4. (Color online) The Binder cumulant for $a = -3$ and different system sizes.

A convolution in real space becomes a multiplication in Fourier space:

$$\tilde{\eta}(\vec{k}) = \tilde{\Phi}(\vec{k})\tilde{u}(\vec{k}). \tag{5}$$

Now insert Eq. (5) into Eq. (4) to determine the convolution kernel:

$$N\tilde{\mathcal{C}}(\vec{k}) = \langle \tilde{\Phi}(\vec{k})\tilde{u}(\vec{k})\tilde{\Phi}^*(\vec{k})\tilde{u}^*(\vec{k})\rangle = |\tilde{\Phi}(\vec{k})|^2\langle|\tilde{u}(\vec{k})|^2\rangle. \tag{6}$$

We choose the real-space random numbers $u(\vec{x})$ as being iid according to a Gaussian with zero mean and variance 1,

$$\langle u(\vec{x})\rangle = 0, \tag{7}$$

$$\langle u(\vec{x})u(\vec{y})\rangle = \delta_{\vec{x},\vec{y}}, \tag{8}$$

such that the variance $\langle|\tilde{u}(\vec{k})|^2\rangle = N$. This results in $\tilde{\mathcal{C}}(\vec{k}) = |\tilde{\Phi}(\vec{k})|^2$, so we can calculate the correlated random numbers in the Fourier space from

$$\tilde{\eta}(\vec{k}) = \sqrt{\tilde{\mathcal{C}}(\vec{k})}\tilde{u}(\vec{k}). \tag{9}$$

The back-transformed correlated random numbers $\eta(\vec{r})$ are real numbers. Since $u(\vec{r}) \in \mathbb{R}$ it follows that $\tilde{u}(-\vec{k}) = \tilde{u}^*(\vec{k})$. From Eq. (4) we infer $\tilde{\mathcal{C}}(\vec{k}) = \tilde{\mathcal{C}}(|\vec{k}|) \in \mathbb{R}^+$. So the back transformation $\eta(\vec{r}) = \mathcal{F}^{-1}[\tilde{\eta}(\vec{k})](\vec{r}) \in \mathbb{R}$.

For maximum flexibility, to test different types of correlation function, we have implemented the Fourier transformation numerically, using the "Fastest Fourier Transform in the West" (FFTW) library, version 3.2.2.[26] An example of a realization of the correlated disorder is shown in Fig. 1 for different values of a.

We tested our procedure by generating 20 realizations for $a = -1$ of the correlated disorder, calculating the two-point correlation Eq. (2) directly, and fitting Eq. (3) with variable exponent a. The correlation, shown in Fig. 2, and the resulting value $a = 1.003(2)$ show that, except for very small correlations at large distances, the procedure works very well.

Next, we mention briefly how the exact ground states are calculated. The phase space of the uncorrelated RFIM consists of a ferromagnetic and a paramagnetic phase (see Fig. 3). The transition from one phase to the other can be triggered by varying the disorder strength h or the temperature T. Change of both along a path $f(h,T)$ in the phase space leads to a critical point $P_c = (h_c, T_c)_{f(h,T)}$. From renormalization group calculations, the RFIM is known[27] to exhibit the same critical behavior at any P_c, except for the temperature-driven phase transition point of the standard nonrandom Ising model. This allows us to focus on $T = 0 = \text{const}$ and vary just h, to study the critical behavior along the full transition line. We do not know *a priori* whether the phase diagram for the correlated-disorder case has the same property; nevertheless, it makes sense to concentrate, at least for our study presented here, also on $T = 0$. From the computational point of view this is very favorable, since it is possible to calculate exact ground states at $T = 0$ in a very efficient way for system sizes as large as $N = 141^3$ spins. Within this approach,[28,29] each realization of the correlated net fields $(\{\eta_i\}, H)$ has to be mapped to a graph with $N + 2$ nodes and $2N + 1$ edges

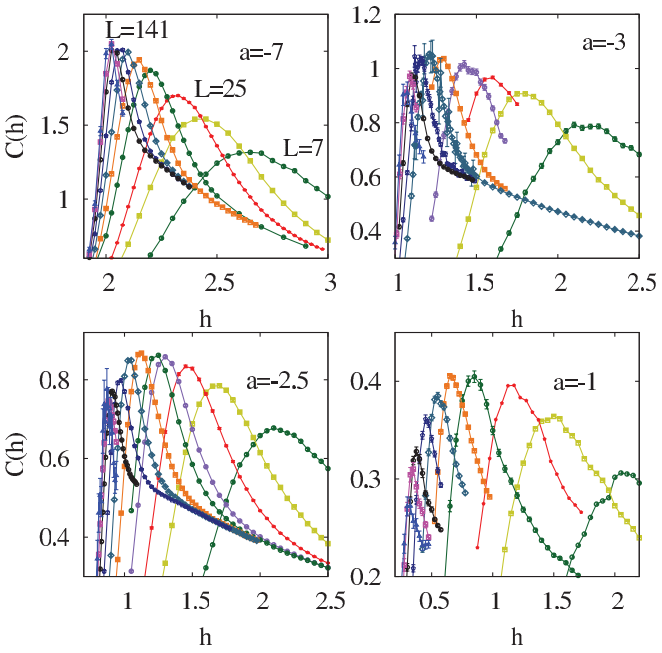

FIG. 5. (Color online) Specific-heat-like quantity for different correlation exponents $a = -7$ to -1 and system sizes $L = 7, 11, 15, 21, 25, 35, 49, 69, 97, 117$, and 141. For all values of a the curves appear in monotonic ordering, meaning the curve of $L = 7$ is on the very right and $L = 141$ is on the very left, as labeled on the upper left subplot. The lines are guides to the eyes only.

TABLE II. Fit parameters of Eq. (21) for the peak position of the specific-heat-like quantity. The upper part contains the parameters for finite h_c. For the lower part $h_c = 0$ was fixed.

	$a = -7$	$a = -3$	$a = -2.5$	$a = -2$	$a = -1$
h_c	1.962(4)	0.992(8)	0.73(1)	0.537(8)	0.183(9)
f	3.2(1)	6.0(3)	6.0(3)	7.5(2)	9.8(3)
$1/\nu$	0.79(2)	0.84(2)	0.76(2)	0.81(2)	0.84(2)
Assuming no critical point $\Leftrightarrow h_c = 0$					
f_0	2.62(5)	2.61(8)	3.0(2)	3.1(1)	5.5(3)
$1/\nu_0$	0.055(5)	0.187(8)	0.27(2)	0.32(1)	0.58(1)

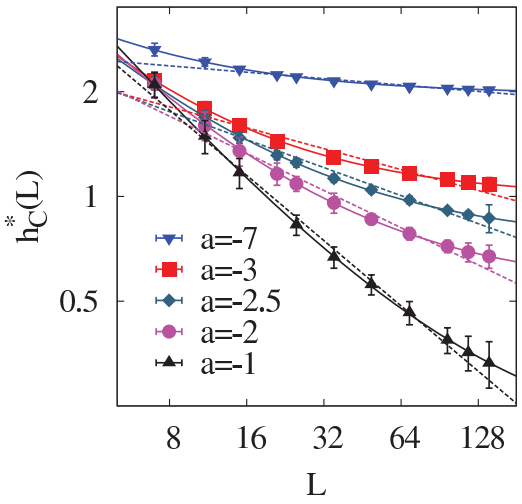

FIG. 6. (Color online) Peak positions of the specific-heat-like quantity as functions of the system sizes for $a = -7$ to -1. The solid lines are fits assuming a finite critical value according to Eq. (21); the broken ones are fits with $h_c = 0$.

with suitable edge capacities. On this graph a sophisticated maximum-flow–minimum-cut algorithm can be applied.[30,31] The resulting minimum cut directly corresponds to the ground state (GS) spin configuration $\{S_i\}$ of that specific realization of the net disorder. We used the efficient maximum-flow subroutines implemented in the LEDA library.[32]

III. QUANTITIES OF INTEREST

From a GS spin configuration, some quantities of interest can be obtained directly, such as the magnetization per spin

$$M = \frac{1}{N}\sum_{i}^{N} S_i \tag{10}$$

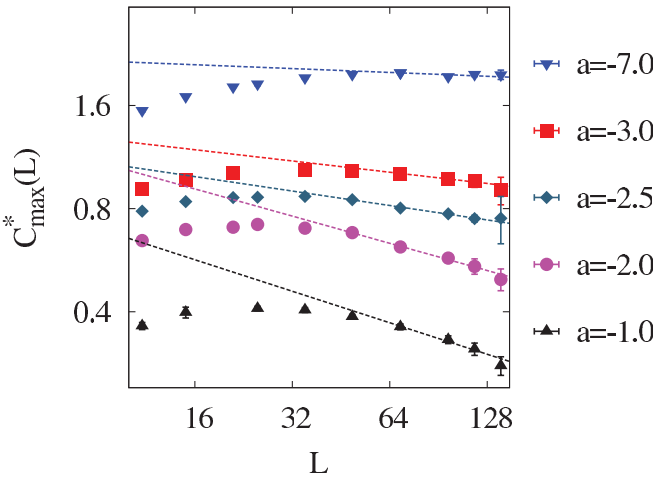

FIG. 7. (Color online) Peak heights of the specific heat as functions of the system size for $a = -7$ to -1. The lines are fits assuming a power-law decay for large system sizes.

TABLE III. Fit parameters of Eq. (23) for the height of the maxima of the specific heat as shown in Fig. 7.

	$a=-7$	$a=-3$	$a=-2.5$	$a=-2$	$a=-1$
k	2.3(2)	1.6(1)	1.46(2)	1.9(1)	1.3(2)
α/ν	−0.04(2)	−0.11(2)	−0.140(7)	−0.26(1)	−0.31(4)

and the bond energy per spin

$$E_J = -\frac{J}{N}\sum_{\langle i,j\rangle} S_i S_j. \tag{11}$$

Note that the thermal expectation value $\langle E_J\rangle$ is the derivative of the free energy per spin with respect to the coupling constant J.

Using these individual values, we calculate averaged quantities like the average magnetization $m = \langle M\rangle$. This disorder average $\langle\cdots\rangle$ is performed always for a fixed value of h. We also consider the Binder cumulant[33]

$$g(h,L) = \frac{1}{2}\left(3 - \frac{\langle M^4\rangle}{\langle M^2\rangle_h^2}\right). \tag{12}$$

A specific-heat-like quantity $C(h)$ can be calculated as the numerical derivative of E_J with respect to h. The expectation value $\langle C(h)\rangle$ is a twofold derivative of the free energy and should be comparable to the real specific heat in its critical behavior. An exact analytic relation of the specific heat and $C(h)$ is not possible for $T = 0$. Nevertheless, the reason to use $C(h)$ here is that, when measuring the critical behavior, one has to vary some parameter so as to cross the critical line, which is the case here when J or h is varied. Note that one could also study the twofold derivative with respect to h (the first derivative of the free energy is the expectation value of the field energy); one would always recover the same critical behavior (see Ref. 6 for details). And indeed, for uncorrelated

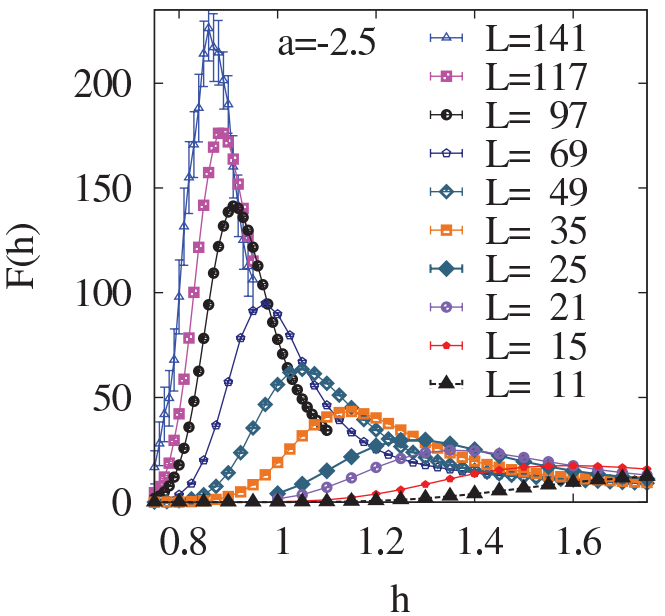

FIG. 8. (Color online) Fluctuation of the bond energy for $a = -2.5$ and different system sizes. Lines are guides to the eyes only.

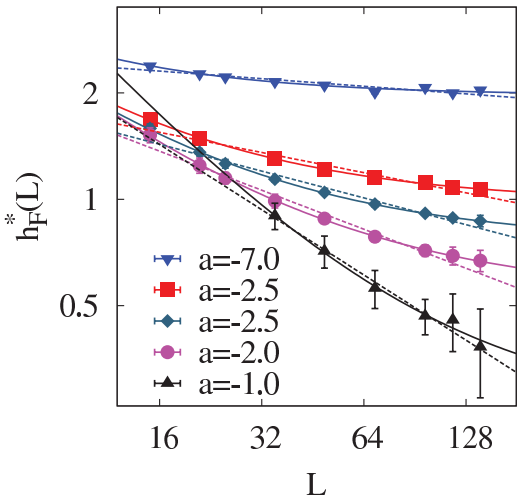

FIG. 9. (Color online) Peak positions of the fluctuation of the bond energy as functions of the system size for $a = -7$ to -1. The lines are fits according to Eq. (21).

disorder, at $T = 0$ the same behavior of $C(h)$ was found as for the real specific heat in Monte Carlo simulations. Hence, from here on we will refer to $C(h)$ sometimes as the specific heat,

$$C(h) = \frac{\langle \partial E_J(h) \rangle}{\partial h}. \tag{13}$$

Furthermore, we study the fluctuations of the bond energy,

$$F(h) = N\left(\langle E_J^2 \rangle - \langle E_J \rangle^2\right). \tag{14}$$

Note that this quantity is not directly related to the specific heat, since the average $\langle \cdots \rangle$ over the disorder is a linear operation for all physical quantities. In any case, it resembles the temperature-ensemble fluctuations that occur in the calculation of the specific heat in Monte Carlo simulations.

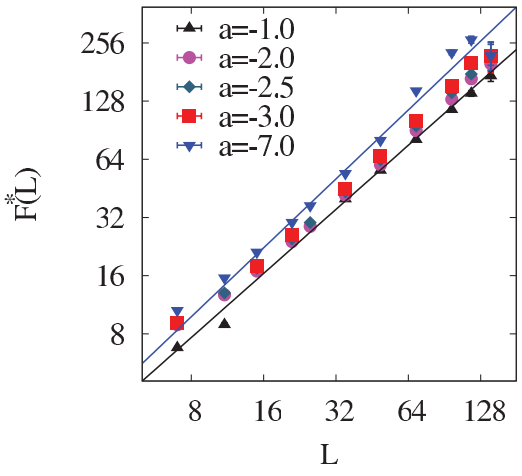

FIG. 10. (Color online) Peak heights of the fluctuation of the bond energy as function of the system size for $a = -7$ to -1. The lines are fits according to Eq. (20) in the range of $L = [15,141]$ for $a = -7.0$ and $a = -1.0$.

TABLE IV. Fit parameters of Eq. (21) for the peak position of the fluctuation of the bond energy. The upper part contains the parameters for finite h_c. For the lower part $h_c = 0$ was fixed.

	$a = -7$	$a = -3$	$a = -2.5$	$a = -2$	$a = -1$
h_c	1.98(2)	1.02(2)	0.78(1)	0.58(2)	0.25(7)
f	8(3)	13(2)	10.9(9)	16(3)	28(20)
$1/\nu_f$	1.1(1)	1.08(6)	0.96(3)	1.04(6)	1.1(2)
Assuming no critical point $\Leftrightarrow h_c = 0$					
f_0	2.9(1)	2.9(3)	3.1(3)	4.4(5)	8(1)
$1/\nu_{f_0}$	0.08(1)	0.21(3)	0.27(2)	0.41(3)	0.61(3)

We also calculate the zero-temperature susceptibility

$$\chi(h) = \left.\frac{\partial m(h,H)}{\partial H}\right|_{H=0} \tag{15}$$

as the linear response of the magnetization to small homogeneous magnetic fields H. Therefore, we apply small homogeneous fields at equidistant values $H_1, 2H_1, 3H_1$ and fit parabolas as functions of H to the magnetizations $m(h, H = 0)$, $m(h,H_1)$, $m(h,2H_1)$, and $m(h,3H_1)$. For a fixed value of the disorder strength h the linear coefficient corresponds to the susceptibility $\chi(h)$.

We will see that the results are compatible with second-order phase transitions, such that the measured quantities show power-law behavior close to the phase transition point. To determine or test the critical exponents, we use the standard scaling forms, i.e.,

$$g(h,L) = \tilde{g}[(h - h_c)L^{1/\nu}], \tag{16}$$
$$m(h,L) = L^{-\beta/\nu}\tilde{m}[(h - h_c)L^{1/\nu}], \tag{17}$$
$$\chi(h,L) = L^{\gamma/\nu}\tilde{\chi}[(h - h_c)L^{1/\nu}], \tag{18}$$
$$C(h,L) = L^{\alpha/\nu}\tilde{C}[(h - h_c)L^{1/\nu}], \tag{19}$$

and apply a finite-size-scaling analysis. For the Binder cumulant and the magnetization we use a nice tool which performs data collapses automatically.[34] It is based on a simplex algorithm and is written in PYTHON.

We assume the same kind of scaling for the fluctuations of the bond energy:

$$2F(h,L) = L^{\kappa/\nu}\ \tilde{F}[(h - h_c)L^{1/\nu}]. \tag{20}$$

The specific heat and the susceptibility show a maximum close to the critical point at some argument f of the universal functions $\tilde{\chi}(\cdot)$ and $\tilde{C}(\cdot)$. Note that the peak positions for specific heat and susceptibility of the same system size L usually differ. Thus, the value of f (and even the sign) may also differ. From Eqs. (18) and (19) it follows that the finite-size

TABLE V. Fit parameters of Eq. (20) for the heights of the maxima of the fluctuation of the bond energy as shown in Fig. 10.

	$a = -7$	$a = -3$	$a = -2.5$	$a = -2$	$a = -1$
f_1	0.8(1)	0.87(5)	0.89(4)	1.06(7)	0.77(8)
κ	1.18(4)	1.16(2)	1.10(1)	1.04(2)	1.10(3)

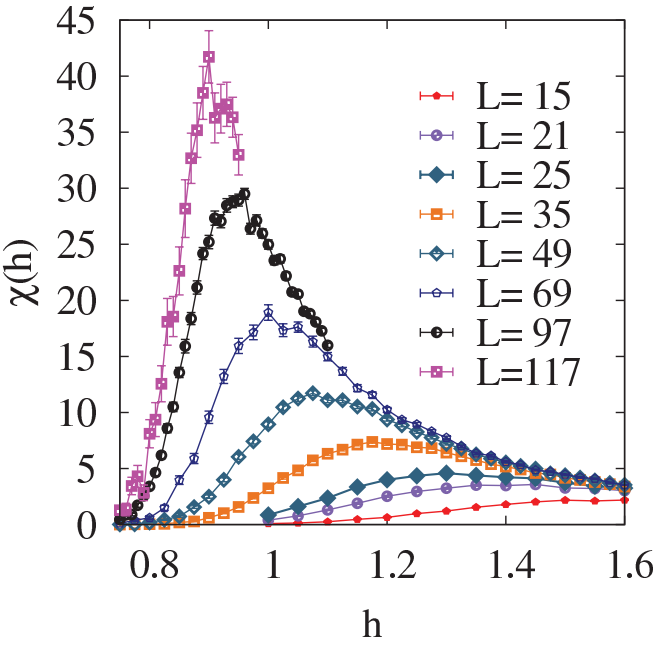

FIG. 11. (Color online) Susceptibility for $a = -2.5$ and different system sizes. Lines are guides to the eyes only.

dependence of the positions of the maxima, respectively, scale as

$$h^*(L) = h_c + fL^{-1/\nu}. \tag{21}$$

When fitting our data, we have also tested for simple power-law corrections to scaling by considering the modified equation

$$h^*(L) = h_c + fL^{-1/\nu}(1 + gL^{-\omega}), \tag{22}$$

where ω is the correction exponent. Also, it follows from Eqs. (18) and (19) that, right at $h^*(L)$, the heights of the maxima should scale as $L^{\gamma/\nu}$ and $L^{\alpha/\nu}$, respectively. In the case of $\alpha = 0$ other forms like a logarithmic divergence or a convergence to a constant ("cusp") have been reported in the

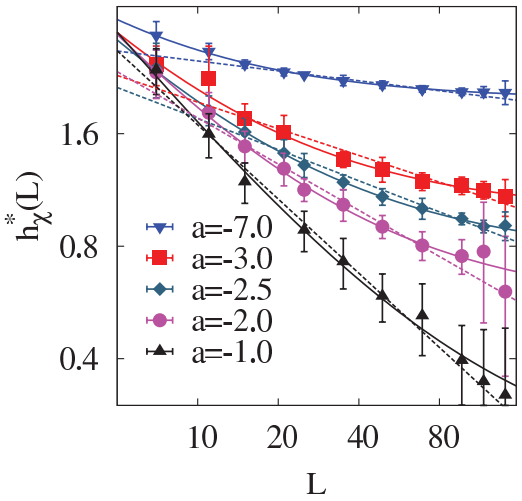

FIG. 12. (Color online) Peak positions of the susceptibility as functions of the system size for $a = -7$ to -1. The solid lines are fits assuming a finite critical value according to Eq. (21); the broken ones are fits imply $h_c = 0$.

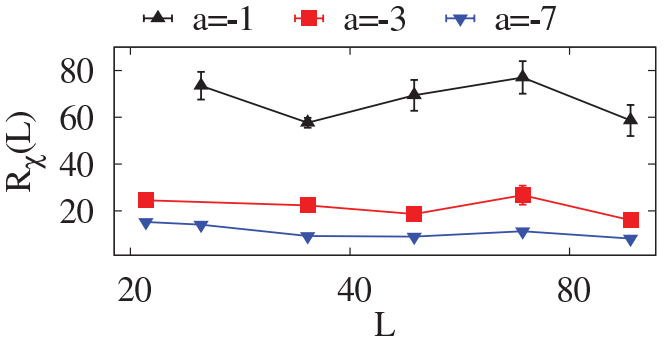

FIG. 13. (Color online) Ratio $R_\chi(L)$ for $a = -7, -3 - 1$. The data points for $a = -2$ lie between those for $a = -7$ and $a = -3$ and are not included for better visibility.

literature for other systems.[6,35] Below we present the results we obtained for the positions and the heights of the peaks and test their scaling behavior according to these scaling assumptions.

As mentioned above, these quantities are average values. They are strongly dependent on the set of disorder realizations taken into account. Hence, we perform an average usually over many thousands of realizations. We estimate the variability of these average values from 200 bootstrap samples[36,37] and quote it as statistical error.

IV. RESULTS

We performed exact ground-state calculations for three-dimensional RFIMs for correlation exponents $a = \{-1.0, -2.0, -2.5 - 3.0, -7.0\}$. We considered system sizes ranging from $L = 7$ to $L = 141$. The number of disorder realizations per system size and per value of the correlation exponent can be found in Table I. The actual number of calculated ground states is four times larger, since four different external fields are needed to obtain a susceptibility. The values of H_1 are stated in the rightmost column of Table I.

Since the Binder cumulant exhibits no clear crossing (see Fig. 4), one might suspect that no phase transition is present. This is not the case as we will see in the following. To determine the phase transition points, we start by considering the average specific heat. In Fig. 5 the results can be seen for $a = -7$ to -1. As for the uncorrelated RFIM, peaks can be observed clearly, which give evidence for the existence of a phase transition for the correlated case also. We estimate the peaks by fitting parabolas over different intervals close to the maximum (for every bootstrap sample). The positions of the peaks in Fig. 5

TABLE VI. Fit parameters of Eq. (21) for the peak position of the susceptibility. The upper part contains the parameters for finite h_c. For the lower part $h_c = 0$ was fixed.

	$a = -7$	$a = -3$	$a = -2.5$	$a = -2$	$a = -1$
h_c	1.97(1)	0.98(4)	0.75(2)	0.56(4)	0.20(5)
f	4.8(5)	7(1)	7.6(6)	9(1)	11(2)
$1/\nu$	0.83(5)	0.84(8)	0.80(4)	0.85(7)	0.88(8)
Assuming no critical point $\Leftrightarrow h_c = 0$					
f_0	3.06(8)	3.4(3)	3.3(3)	4.5(4)	7.7(7)
$1/\nu_0$	0.088(7)	0.24(2)	0.28(2)	0.41(3)	0.66(3)

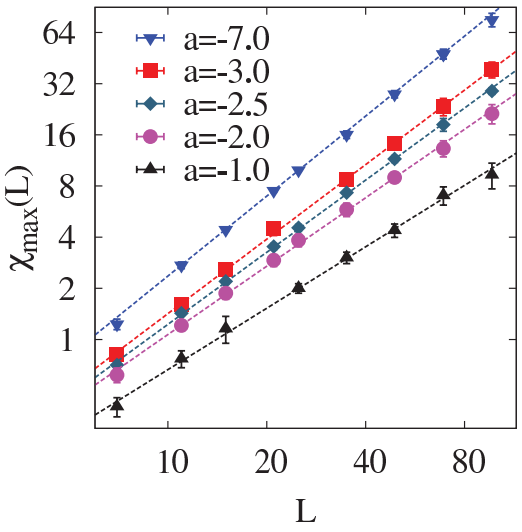

FIG. 14. (Color online) Peak heights of the susceptibility as functions of the system size for $a = -3$ to -1.

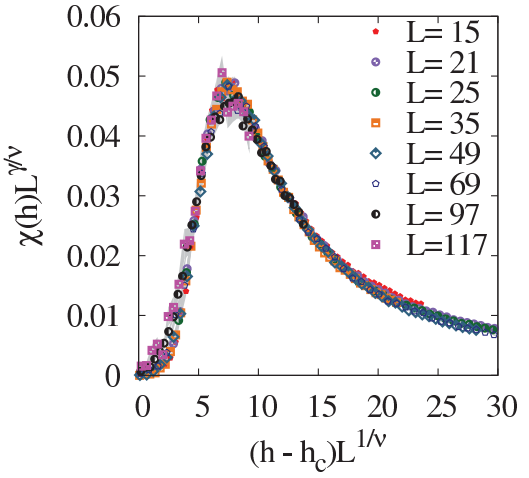

FIG. 15. (Color online) Data collapse of the susceptibility for $a = -2.5$.

move from right to left for increasing system sizes. To obtain the infinite-size limiting value h_c and an estimate for the critical exponent ν of the correlation length, we fit the positions of the peaks to Eq. (21), resulting in fit values as shown in the upper part of Table II. Note that when determining the error bars from model fitting, we usually have not only taken the statistical error obtained from the fit routine (of the GNUPLOT program) but always also varied the range of sizes, to get an impression of possible systematic errors.

In Fig. 5 for the case $a = -1$, the peaks move very close to $h = 0$ and the result from the fit for h_c is also close to zero. Therefore, another sensible ansatz is to set $h_c = 0$. Fit parameters for this ansatz are also shown in Table II in the lower part. Both models are plotted in Fig. 6 as solid and broken lines, respectively. All data sets exhibit some curvature, indicating that $h_c > 0$. Nevertheless, for $a \geqslant -2$, the data points within error bars are also compatible with a pure power law. In particular, if one includes corrections to scaling according to Eq. (22) using $h_c \equiv 0$, fits with a very high quality for $a \geqslant -2$ were obtained. On the other hand, for $a < -2$ a fit with $h_c > 0$ is always better: the leading exponent $(-1/\nu)$ gets close to zero (i.e., the leading term becomes "automatically" almost constant), or even positive (i.e., $\nu < 0$), which shows that the fit is unsuitable. For $a < -2$ the assumption $h_c > 0$ is confirmed, and the results are compatible with the analytical predictions of Nattermann mentioned above.[15]

To determine the critical exponent α according to Eq. (19), we analyzed the peak heights of the specific heat as shown in Fig. 7. They increase up to $L \approx 50$ for all correlation exponents a and decrease for larger L. Thus, no clear scaling is visible. This could be due to very strong finite-size corrections. Therefore, under the assumption that the specific heat decreases in a power-law fashion, we fitted the data points for very large system sizes to a power law of the form

$$C(h, L) = kL^{\alpha/\nu}. \tag{23}$$

The achieved exponents are small and negative. They can be found in Table III. On the other hand, it is possible that the specific heat levels off for even larger system sizes, which would give the leading behavior $\alpha = 0$. In Sec. V, we will discuss these two options in connection with the Rushbrooke inequality[38] and see that $\alpha = 0$ appears to be more likely for $a < -2$, while the data do not allow a definite decision in the strong-correlation case $a \geqslant -2$.

Next, we display the fluctuation of the bond energy. An exemplary plot for $a = -2.5$ is shown in Fig. 8. For all values of the correlation exponent a, we observe such peaks at some value of the disorder strength h. We carried out the usual analysis: We fitted parabolas to the peaks and determined the scaling behavior from the position as a function of the system size (see Fig. 9) and the peak height (Fig. 10). For $a = -1.0$ the peaks are very shallow for small system sizes, so we have excluded them from the analysis of the peak position. The resulting fit parameters are shown in Table IV for the positions and in Table V for the height.

We now turn to the susceptibility. The phase transition is signaled by a divergence of the susceptibility. An increasing peak can be seen for $a = -2.5$ in Fig. 11 as an example. The peaks are estimated in the same way as for the specific heat. The resulting maxima are tuples $(h^*(L), \chi_{max}(L))$ of position and height.

For the peak position of the susceptibility we assumed the same model as we did for the specific heat. The models and data points can be found in Fig. 12. In particular, for $a = -1$, the error bars are quite large, despite the large number of samples, which for the largest system sizes is considerably higher than for the cases $a < -1$. To understand this behavior, we studied the degree of non-self-averaging[39] and calculated

$$R_\chi(L) = \mathrm{var}[\chi(L)]/\langle\chi(L)\rangle^2. \tag{24}$$

TABLE VII. Fit parameters for the peak heights of the susceptibility when fitted according to $b_0 L^{\gamma/\nu}$.

	$a = -7$	$a = -3$	$a = -2.5$	$a = -2$	$a = -1$
b_0	0.064(3)	0.049(2)	0.048(2)	0.049(2)	0.041(3)
γ/ν	1.56(1)	1.45(1)	1.41(1)	1.34(2)	1.20(2)

We found R_χ to stay approximately constant for increasing L, as shown in Fig. 13 for susceptibility measured at the peak positions. We found the same behavior qualitatively for different fixed values of h, which shows that the correlated RFIM is non-self-averaging for a large range of the disorder parameter, like many other systems exhibiting quenched disorder. In particular, the results in Fig. 13 show that the degree of non-self-averaging is strongest for $a = -1$, which explains the large error bars. To achieve much smaller error bars for the susceptibility, a much larger number of samples would be necessary, which is beyond the capacity of our numerical resources.

For the finite-size scaling of the peak positions, we tested Eq. (21) using the saturating ansatz (h_c included in the fit) as well as a pure power-law decay (via $h_c \equiv 0$). The fit parameters for both models can be found in Table VI. Again the saturating model brings up, within the present accuracy, the same infinite-size critical point h_c as we found before. And again, for values $a \geqslant -2$, $h_c = 0$ is also compatible with the numerical results.

In contrast to the specific heat, the peak heights of the susceptibility show a clear power-law behavior for all studied correlation exponents (see Fig. 14). Thus, in the thermodynamic limit the susceptibility diverges. Compared to the peak positions displayed in Fig. 12, the fluctuations for the peak height here are much smaller; thus a clear power-law behavior is visible. The critical exponents γ/ν, as obtained from a power-law fit, are displayed in Table VII. The values decrease with increasing a. The fit parameters obtained can be used to collapse the susceptibility according to Eq. (17) with satisfactory agreement. As an example, we show the collapsed susceptibility for $a = -2.5$ in Fig. 15.

For a finite-size analysis of the Binder cumulant and of the magnetization, we performed data collapses according to Eqs. (16) and (17). Example data collapses for the magnetization and as inset for the Binder cumulant for $a = -3$ are shown in Fig. 16. The quality of the collapses is very good. They lead to sets of critical values and exponents as shown in Table VIII. Furthermore, for $a = -2$ and -1, we have also performed data collapses for the magnetization when fixing $h_c \equiv 0$. For $a = -1$ such a data collapse is possible, leading

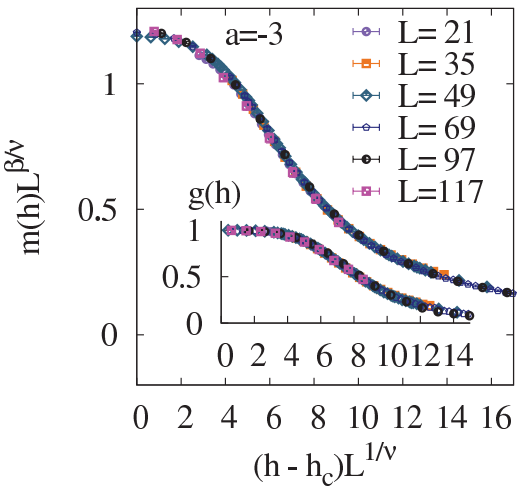

FIG. 16. (Color online) Data collapse of the magnetization and of the Binder cumulant (inset) for $a = -3$.

TABLE VIII. Critical value h_c and correlation length exponent ν derived from the finite-size-scaling analysis of the Binder cumulant and the magnetization.These values are obtained via data collapses. The three smallest system sizes, i.e., $L = 7,11,15$, are left out of the data collapses for $a = -2.5$.

	$a=-7$	$a=-3$	$a=-2.5$	$a=-2$	$a=-1$
h_c	1.94(1)	0.95(2)	0.731(2)	0.47(4)	0.12(3)
$1/\nu$	0.78(2)	0.77(4)	0.74(3)	0.75(3)	0.78(4)
β/ν	0.005(5)	0.03(2)	0.01(1)	0.01(1)	0.01(8)

to $\beta/\nu = 0.08(4)$. However, for $a = -2$, the quality of the collapse with $h_c \equiv 0$ is very bad, even for the Binder cumulant (neither shown here), which seems to indicate that $h_c = 0$ is less likely compared to $h_c > 0$.

V. CONCLUSIONS AND DISCUSSION

We have presented the results of exact ground-state calculations, i.e., calculations in thermal equilibrium, for the RFIM with power-law-correlated disorder for different correlation exponents. To calculate the ground states numerically, we have applied a mapping to the maximum-flow problem. Using efficient polynomial-time-running maximum-flow–minimum-cut algorithms, we were able to study large systems sizes up to $N = 141^3$.

We studied different quantities like the magnetization, Binder cumulant, susceptibility, a specific-heat-like quantity, and energy fluctuations, and applied finite-size-scaling techniques to obtain the critical exponents. The combined results for the critical exponents are shown in Table IX. As discussed in the previous section, for large values of the correlation exponent α, in particular $\alpha \geqslant -2$, the large-scale behavior of the specific heat is not clear. It might decrease as a power law, leading to $\alpha < 0$, or it might level off to a constant. We tested the two possibilities for the values of α by considering the Rushbrooke inequality $\alpha + 2\beta + \gamma \geqslant 2$, which holds usually as the equality.[40] When $\alpha = 0$ is chosen, the Rushbrooke equation is satisfied in all cases within error bars. For the values of α quoted in Table III, obtained via fitting the data for just the few largest system sizes, the Rushbrooke sum (assuming $h_c > 0$) is considerably smaller than 2 for $a = -2, -1$. Hence, the value $\alpha = 0$ appears to be more likely. Furthermore, it is not clear to us whether the specific-heat-like quantity $C(h)$, which reproduces the scaling behavior of the real specific heat

TABLE IX. Final results for the value of h_c, the critical exponents α, β, γ, and ν, and the Rushbrooke (RS) sum $\alpha + 2\beta + \gamma$. The first row ($a = -\infty$) shows the result for the uncorrelated case taken from Refs. 6 and 7. The row -1^* is for the assumption $h_c(a = -1) = 0$.

a	h_c	α	β	γ	ν	RS sum
$-\infty$	2.27(1)	~ 0	0.016(7)	2.1(1)	1.37(9)	2.1(2)
-7.0	1.96(2)	0	0.01(1)	2.0(3)	1.26(8)	2.0(3)
-3.0	0.97(2)	0	0.04(6)	1.8(4)	1.2(2)	1.8(5)
-2.5	0.74(2)	0	0.01(1)	1.91(8)	1.3(5)	1.93(9)
-2.0	0.52(5)	0	0.01(3)	1.7(3)	1.2(2)	1.7(4)
-1.0	0.17(5)	0	0.05(10)	1.5(3)	1.2(2)	1.5(5)
-1^*	0	0	0.1(1)	1.9(1)	1.61(9)	2.0(2)

well for the uncorrelated case, is still useful, in particular in the case of strong correlations. The peculiar behavior for large systems might be due to this.

In all cases, the values quoted in Table IX are compatible within error bars with the results for the uncorrelated case, in particular due to the relatively large error bar for the critical exponent γ. Nevertheless, the data for the peak heights of the susceptibility (Fig. 14) show a trend toward a smaller slope when a increases from -7 to -1: The results for γ/ν, which exhibit a small error bar (see Table VII) are clearly different within error bars; in particular, the values for $a \geqslant -3$ are different from the value of γ/ν for $a = -7$, which within error bars is equal to the value for the uncorrelated case. In this case, to still satisfy the Rushbrooke inequality, the true value for ν, in particular for values $a = -2$ and -1, should be larger, at or somewhat above the upper bounds, given the standard error bars. Hence, it is quite likely that the correlation of the disorder creates nonuniversality for the RFIM, as in the case of the diluted ferromagnet.[17] This is compatible with Nattermann's calculation,[15] in which the behavior might change for $a \geqslant -d$.

In that work, Nattermann also predicted that the long-range order is destroyed for $a \geqslant -2$. Our results for $a = -1$ clearly allow this; see last row of Table IX. For $a = -2$, from the calculation of the critical value h_c via the scaling of the peaks of the specific heat, from the fluctuations of bond energy, and from the susceptibility, this is possible as well. Nevertheless, the data collapse for the magnetization and Binder cumulant is very bad in the case $a = -2$ when $h_c \equiv 0$ is assumed. Also, the result of $\nu \approx 2.6$ (see, e.g., the last row in Table VI) is quite large under the assumption of $h_c \equiv 0$, which in turn leads to a quite large value of $\gamma = 3.3$, which results in the Rushbrooke sum being much larger than 2, even if we assume $\beta \approx 0$ and $\alpha \approx -0.26 \times 2.6 - 0.68 < 0$. Hence, from our results $h_c(a = -2) > 0$ appears more likely to us. This could be due to the fact that $a = -2$ is exactly the borderline case, such that much higher system sizes might be necessary to see the limiting behavior. This is out of reach with current technology, since we already study tens of thousands of samples with exact algorithms for systems exhibiting up to almost 3×10^6 spins. Nevertheless, it could also be that the Imry-Ma-type argument of Nattermann has to be refined to make it more exact.

ACKNOWLEDGMENTS

We would like to thank K. Janzen for fruitful discussions and a critical reading of the manuscript. Furthermore, we are grateful to M. Niemann and M. Weigel for helpful comments. The calculations were carried out on GOLEM (Großrechner Oldenburg für Explizit Multidisziplinäre Forschung) and HERO (High-End Computing Resource Oldenburg) at the University of Oldenburg.

*bjoern.ahrens@uni-oldenburg.de

[1] J. Bricmont and A. Kupiainen, Phys. Rev. Lett. **59**, 1829 (1987).
[2] M. Gofman, J. Adler, A. Aharony, A. B. Harris, and M. Schwartz, Phys. Rev. Lett. **71**, 1569 (1993).
[3] H. Rieger, Phys. Rev. B **52**, 6659 (1995).
[4] U. Nowak, K. D. Usadel, and J. Esser, Physica A **250**, 1 (1998).
[5] A. K. Hartmann and U. Nowak, Eur. Phys. J. B **7**, 105 (1999).
[6] A. K. Hartmann and A. P. Young, Phys. Rev. B **64**, 214419 (2001).
[7] A. A. Middleton and D. S. Fisher, Phys. Rev. B **65**, 134411 (2002).
[8] C. Frontera and E. Vives, Comput. Phys. Commun. **147**, 455 (2002).
[9] E. T. Seppälä, A. M. Pulkkinen, and M. J. Alava, Phys. Rev. B **66**, 144403 (2002).
[10] A. K. Hartmann, Phys. Rev. B **65**, 174427 (2002).
[11] A. A. Middleton, e-print arXiv:cond-mat/0208182.
[12] M. Zumsande, M. J. Alava, and A. K. Hartmann, J. Stat. Mech. (2008) P02012.
[13] B. Ahrens and A. K. Hartmann, Phys. Rev. B **83**, 014205 (2011).
[14] A. A. Fedorenko and F. Kühnel, Phys. Rev. B **75**, 174206 (2007).
[15] T. Nattermann, J. Phys. C **16**, 6407 (1983).
[16] H. A. Makse, S. Havlin, M. Schwartz, and H. E. Stanley, Phys. Rev. E **53**, 5445 (1996).
[17] H. G. Ballesteros and G. Parisi, Phys. Rev. B **60**, 12912 (1999).
[18] S. Hod and U. Keshet, Phys. Rev. E **70**, 015104 (2004).
[19] A. A. Fedorenko, Phys. Rev. B **77**, 094203 (2008).
[20] A. Weinrib and B. I. Halperin, Phys. Rev. B **27**, 413 (1983).
[21] A. B. Harris, J. Phys. C **7**, 1671 (1974).
[22] H. G. Ballesteros, L. A. Fernndez, V. Martn-Mayor, A. M. Sudupe, G. Parisi, and J. J. Ruiz-Lorenzo, J. Phys. A **32**, 1 (1999).
[23] H. G. Ballesteros, L. A. Fernández, V. Martín-Mayor, A. Muñoz Sudupe, G. Parisi, and J. J. Ruiz-Lorenzo, Phys. Rev. B **58**, 2740 (1998).
[24] C.-K. Peng, S. Havlin, M. Schwartz, and H. E. Stanley, Phys. Rev. A **44**, R2239 (1991).
[25] S. Prakash, S. Havlin, M. Schwartz, and H. E. Stanley, Phys. Rev. A **46**, R1724 (1992).
[26] M. Frigo and S. G. Johnson, Proc. IEEE **93**, 216 (2005), special issue on program generation, optimization, and platform adaptation.
[27] A. J. Bray and M. A. Moore, J. Phys. C **18**, 927 (1985).
[28] J. C. Picard and H. D. Ratliff, Networks **5**, 357 (1975).
[29] A. T. Ogielski, Phys. Rev. Lett. **57**, 1251 (1986).
[30] A. V. Goldberg and R. E. Tarjan, J. ACM **35**, 921 (1988).
[31] A. K. Hartmann and H. Rieger, *Optimization Algorithms in Physics* (Wiley-VCH, Berlin, 2001).
[32] K. Mehlhorn and S. Näher, *The LEDA Platform of Combinatorial and Geometric Computing* (Cambridge University Press, Cambridge, 1999), [http://www.algorithmic-solutions.de].
[33] K. Binder, Z. Phys **43**, 119 (1981).
[34] O. Melchert, e-print arXiv:0910.5403.
[35] J. M. Yeomans, *Statistical Mechanics of Phase Transitions* (Oxford University Press, Oxford, 1993).
[36] B. Efron and R. J. Tibshirani, *An Introduction to the Bootstrap* (Chapman & Hall/CRC, Boca Raton, London, New York, 1993).
[37] A. K. Hartmann, *A Practical Guide To Computer Simulation* (World Scientific, Singapore, 2009).
[38] G. S. Rushbrooke, J. Chem. Phys. **39**, 842 (1963).
[39] S. Wiseman and E. Domany, Phys. Rev. Lett. **81**, 22 (1998).
[40] G. S. Rushbrooke, J. Chem. Phys. **43**, 3439 (1965).